Computers and Mathematics with Applications 59 (2010) 2200–2214

Contents lists available at ScienceDirect

Computers and Mathematics with Applications

journal homepage: www.elsevier.com/locate/camwa

Investigation of the LES WALE turbulence model within the lattice Boltzmann framework

M. Weickert [a,*], G. Teike [a], O. Schmidt [a], M. Sommerfeld [b]

[a] Robert Bosch GmbH, Post Office Box 10 60 50, 70049 Stuttgart, Germany

[b] Martin-Luther-Universität Halle-Wittenberg, Mechanische Verfahrenstechnik, 06099 Halle (Saale), Germany

ARTICLE INFO

Keywords:
Lattice Boltzmann
LES
Turbulence
WALE
Smagorinsky
Van Driest
Channel flow
Wall-mounted cube

ABSTRACT

Turbulence models which can perform the transition from laminar flow to fully developed turbulent flow are of key importance in industrial applications. A promising approach is the LES WALE model, which can be used without wall functions or global damping functions. The model produces an efficient and fast scheme due to its algebraic character. Additionally, its prediction of the transition from laminar to turbulent regimes has shown promising results. In this work, the LES WALE model is investigated within the lattice Boltzmann framework. For validation purposes, various test cases are presented. First, a channel flow at a Reynolds number of 6876 is investigated. Secondly, the flow around a wall-mounted cube at various Reynolds numbers is determined. The flow regime varies from laminar, to transitional, to fully turbulent conditions at a Reynolds number of 40,000 with respect to the cube height.

© 2009 Elsevier Ltd. All rights reserved.

1. Introduction

Large Eddy simulations (LES) provide a very promising approach for the simulation of turbulent flows because computation times are significantly lower than those of Direct Numerical simulations (DNS). Further, their resolution of turbulent structures is more accurate in comparison to Reynolds Averaged Navier–Stokes (RANS) simulations. For many years now, a variety of sub-grid-scale (SGS) models for LES simulations have been detailed in the literature. Unfortunately, these models have led to differing results, depending on the implementation and application [1]. In the context of this work, implementation and investigation of the LES WALE [2], the Smagorinsky [3], and the Smagorinsky–Van Driest [4] SGS model are carried out based on an in-house lattice Boltzmann solver. Three different test cases are investigated. The first test case consists of a channel flow with a channel Reynolds number of 6876. The test cases are validated by comparing the results with a DNS simulation from Moser [5]. The second test case considers the flow around a wall-mounted cube in a channel. The Reynolds number given by the cube height varies between 200 and 2000. The results are validated with a Scale Adaptive Simulation (SAS) [6] performed with ANSYS CFX 11 [7]. The SAS simulation is based on a finite volume algorithm, which solves the Navier–Stokes equations on unstructured grids. The third test case considers the flow in a fully turbulent flow regime at a Reynolds number of 40,000 with respect to the cube height. Results for this flow are compared with experimental data from Martinuzzi [8].

2. MRT lattice Boltzmann method

A D3Q19 Multiple Relaxation Time (MRT) lattice Boltzmann solver is developed in this work. The MRT model is implemented according to the algorithm of d'Humières [9] to stabilize the numerical method. The lattice Boltzmann (LB)

* Corresponding author.
E-mail addresses: mathias.weickert@de.bosch.com (M. Weickert), gerd.teike@de.bosch.com (G. Teike), oliver.schmidt2@de.bosch.com (O. Schmidt), martin.sommerfeld@iw.uni-halle.de (M. Sommerfeld).

0898-1221/$ – see front matter © 2009 Elsevier Ltd. All rights reserved.
doi:10.1016/j.camwa.2009.08.060

Nomenclature

f	Distribution function
g	Square of velocity gradient tensor
C_X	LES model constant
C_S	LES Smagorinsky constant
C_{SD}	LES Smagorinsky–Van Driest constant
C_D	LES Lilly constant
C_W	LES WALE constant
Δt	Time step [s]
Δx	Grid width [m]
e	Discrete lattice velocity
b	Channel width [m]
L	Channel length [m]
h	Channel height [m]
H	Cube height [m]
m	Moment
M	Transformation matrix
$\overline{\varpi}$	LES Model operator
Re	Reynolds number
S	Shear stress tensor
s	Activity parameter
u	Velocity [m/s]
x	Location coordinate [m]
y	Wall gap [m]
y_+	Dimensionless wall gap
u_τ	Dimensionless wall friction
$j^{(0)}$	Equilibrium flow momentum
Z	Diagonal collision matrix

Greek letters

ν_0	Molecular viscosity [$\frac{\mathrm{m}^2}{\mathrm{s}}$]
ν_t	Eddy viscosity [$\frac{\mathrm{m}^2}{\mathrm{s}}$]
ρ	Density [$\frac{\mathrm{kg}}{\mathrm{m}^3}$]
$\rho^{(0)}$	Equilibrium density
κ	Karman constant
Ω	Rotation tensor
τ_0	Molecular relaxation parameter
τ_t	Turbulent relaxation parameter
τ_{total}	Total relaxation parameter

Indices

i, j, k	Loop variable
b	Bulk
R	Reichardt
n, N	Number

equation (1) is given in discrete formulation in momentum space as:

$$\mathbf{f}(t + \Delta t, \boldsymbol{x} + \boldsymbol{e}_i \Delta t) - \mathbf{f}(t, \boldsymbol{x}) = -\mathsf{M}^{-1} \cdot \mathsf{Z} \cdot \left[\mathbf{m}(t, \boldsymbol{x}) - \mathbf{m}^{(0)}(t, \boldsymbol{x})\right], \tag{1}$$

where the bold-faced symbols denote $(N + 1)$-tuple vectors for a model of $(N + 1)$ discrete velocities, e.g.,

$$\mathbf{f}(t, \boldsymbol{x}) \equiv (f_0(t, \boldsymbol{x}), f_1(t, \boldsymbol{x}), \ldots, f_N(t, \boldsymbol{x}))^{\mathsf{T}}, \tag{2}$$

where T denotes the transpose operator.

In Eq. (1), Δt is the lattice time step, t indicates the time, $\boldsymbol{x}$ denotes the space coordinates, and $\boldsymbol{e}_i$ is the discrete lattice velocity in direction i. The diagonal collision matrix Z is

$$\mathsf{Z} \equiv \mathrm{diag}(s_0, s_1, \ldots, s_{18}), \tag{3}$$

with relaxation rates s_i.

The equilibrium distribution functions in velocity space $\{f_i^{(0)} | i = 0, 1, \ldots, 18\}$ are defined as follows:

$$f_i^{(0)} = \omega_i \rho \left[1 + \frac{3}{c^2} \boldsymbol{e}_i \cdot \boldsymbol{u} + \frac{9}{2c^4} (\boldsymbol{e}_i \cdot \boldsymbol{u})^2 - \frac{3}{2c^2} \boldsymbol{u}^2 \right], \tag{4}$$

where ω_i is a weighting factor chosen as $\omega_0 = 1/3$, $\omega_i = 1/18$ for $i = 1, 2, \ldots, 6$, and $\omega_i = 1/36$ for $i = 7, 8, \ldots, 18$, ρ is the fluid density, $c = \Delta x / \Delta t$, and $\boldsymbol{u}$ is the lattice fluid velocity.

Transformation of the equilibrium values of the distribution functions $\mathbf{f}^{(0)}$ to moment space $\mathbf{m}^{(0)}$ are performed by the matrix M via:

$$\mathbf{m}^{(0)} = \mathsf{M} \cdot \mathbf{f}^{(0)} \tag{5}$$

with

$$\mathbf{m}^{(0)} = (m_0^{(0)}, m_1^{(0)}, \ldots, m_{18}^{(0)})^{\mathsf{T}} \tag{6}$$

and

$$\mathbf{f}^{(0)} = (f_0^{(0)}(t, \boldsymbol{x}), f_1^{(0)}(t, \boldsymbol{x}), \ldots, f_{18}^{(0)}(t, \boldsymbol{x}))^{\mathsf{T}}. \tag{7}$$

The equilibria of the moments are:

$$m_0^{(0)} = \rho, \qquad m_1^{(0)} = -11\rho + \frac{19}{\rho_0} \boldsymbol{j} \cdot \boldsymbol{j}, \qquad m_2^{(0)} = -\frac{475}{63} \boldsymbol{j} \cdot \boldsymbol{j} \tag{8}$$

$$m_3^{(0)} = j_x, \qquad m_5^{(0)} = j_y, \qquad m_7^{(0)} = j_z \tag{9}$$

$$m_4^{(0)} = -\frac{2}{3} j_x, \qquad m_6^{(0)} = -\frac{2}{3} j_y, \qquad m_8^{(0)} = -\frac{2}{3} j_z \tag{10}$$

$$m_9^{(0)} = \frac{1}{\rho_0} \left[2j_x^2 - \left(j_y^2 + j_z^2 \right) \right], \qquad m_{11}^{(0)} = \frac{1}{\rho_0} \left[j_y^2 - j_z^2 \right] \tag{11}$$

$$m_{13}^{(0)} = \frac{1}{\rho_0} j_x j_y, \qquad m_{14}^{(0)} = \frac{1}{\rho_0} j_y j_z, \qquad m_{15}^{(0)} = \frac{1}{\rho_0} j_x j_z \tag{12}$$

$$m_{10}^{(0)} = m_{12}^{(0)} = m_{16}^{(0)} = m_{17}^{(0)} = m_{18}^{(0)} = 0, \tag{13}$$

where ρ_0 is the mean density, $\rho \equiv \sum_{i=0}^{18} f_i$ denotes the density, and $\boldsymbol{j} \equiv \rho \boldsymbol{u}$ is the flow momentum.

An octree-based data structure is implemented according to the algorithm of Crouse [10]. This data structure allows local grid refinements on hierarchical grids.

3. LES models

In LES simulations, an additional viscosity, called the turbulent eddy viscosity ν_t, is introduced in order to model the turbulence. This eddy viscosity is given by:

$$\nu_t = C_X^2 \, \Delta x^2 \, \overline{\varpi}, \tag{14}$$

where C_X denotes the LES model dependent constant, Δx the lattice spacing, and $\overline{\varpi}$ the LES model operator. In the lattice Boltzmann model, the viscosity is related to the relaxation time τ by:

$$\nu_{\text{total}} = \nu_0 + \nu_t = \frac{2\tau_0 - 1}{6} + \frac{\tau_t}{3} \tag{15}$$

where ν_0 is the molecular viscosity. In analogy to splitting up the viscosity term, the relaxation time τ is divided into a molecular and a turbulent part. The total relaxation time is defined as:

$$\tau_{\text{total}} = 3\nu_{\text{total}} + \frac{1}{2}. \tag{16}$$

By applying Eq. (14), we arrive at:

$$\tau_{\text{total}} = 3(\nu_0 + (C_X^2 \Delta x^2) \, \overline{\varpi} \,) + \frac{1}{2}. \tag{17}$$

The total relaxation parameter τ_{total} is derived from the operator $\overline{\varpi}$, which depends on the LES model and is a function of the shear stress tensor S and the rotation tensor Ω.

The shear stress tensor S for Newtonian fluids is defined as

$$S_{i,j} = \nu_0 \rho \left(\frac{\partial \overline{u}_i}{\partial x_j} + \frac{\partial \overline{u}_j}{\partial x_i} \right) \tag{18}$$

and the rotation tensor Ω for Newtonian fluids is given by

$$\Omega_{i,j} = \nu_0 \rho \left(\frac{\partial \overline{u}_i}{\partial x_j} - \frac{\partial \overline{u}_j}{\partial x_i} \right). \tag{19}$$

In this work, a central difference scheme is applied to compute the shear stress tensor S and the rotation tensor Ω. Using the lattice Boltzmann units for the operator $\overline{\varpi}$ and the scaling $\Delta x = \Delta t = 1$, the turbulent relaxation parameter τ_t is obtained:

$$\tau_t = \frac{\sqrt{\tau_0^2 + \frac{18\, C_X^2\, \overline{\varpi}^{\frac{1}{2}}}{\rho}} - \tau_0}{2}. \tag{20}$$

Hou [11] was the first to derive the LES approach for the lattice Boltzmann scheme. In this formulation, only the shear stress tensor S was taken into account, which corresponds to the Smagorinsky model.

3.1. Smagorinsky model

The well-known fine structure model was found by Smagorinsky [3] in 1963. He derived the operator $\overline{\varpi}$ exclusively from the shear stress tensor as follows:

$$\overline{\varpi} = \sum_{i,j} S_{i,j} S_{i,j}. \tag{21}$$

The LES model constant $C_X \equiv C_S$ depends on the application and normally varies between 0.05 and 0.16. Today, this model is commonly used in the literature. Hou was the first to implement the Smagorinsky model in the lattice Boltzmann framework [11]. Krafczyk applied it to the 3D MRT lattice Boltzmann scheme [12]. However, problems appear because the eddy viscosity remains positive even in laminar flows, while it is clear from the definition that ν_t is zero. Moreover, it is shown in [2] that in Smagorinsky's formulation, the wall boundary law is not fulfilled.

3.2. Smagorinsky–Van Driest model

In the Smagorinsky–Van Driest model [4], the LES model constant in Eq. (14) is adjusted to:

$$C_X \equiv C_{SD} = \left[C_D \Delta x \left(1 - \exp^{\frac{-y_+}{A}}\right) \right]^2 \tag{22}$$

with the Van Driest constant $A = 25$, and the Lilly constant $C_D = 0.17$.

It has been proven that the extended Smagorinsky model gives a more precise description of the wall boundary layer [2]. One disadvantage of this approach is the global dependence of the damping function on the dimensionless wall distance.

3.3. WALE model

The WALE model [2] is based on the square of the velocity gradient tensor, which takes into account the shear stress tensor as well as the rotation tensor. The operator $\overline{\varpi}$ is defined as follows:

$$\overline{\varpi} = \frac{(g^d_{i,j} g^d_{i,j})^{\frac{3}{2}}}{(S_{i,j} S_{i,j})^{\frac{5}{2}} + (g^d_{i,j} g^d_{i,j})^{\frac{5}{4}}} \tag{23}$$

with

$$g^d_{i,j} = S_{i,k} S_{k,j} + \Omega_{i,k} S_{k,j} - \frac{1}{3} \delta_{i,j} (S^2 - \Omega^2). \tag{24}$$

Here, the LES model constant C_X of Eq. (14) is set to $C_X \equiv C_W = 0.5$, as proposed by Nicoud [2]. This method keeps the condition of the y^3 near-wall scaling for the eddy viscosity without dynamical algorithms or damping functions. In addition, Nicoud shows that the model can handle transition regimes.

3.4. Dynamic Smagorinsky model

In the dynamic model, the LES constant varies not only in space, but also in time. Therefore, two different filters are recommended [13]. The permanent changing of the LES model can lead to an unstable numerical system, as shown in [14]. For this reason, the dynamic model is not further investigated in this work.

4. Test cases

In this work, the progression from an academic investigation of a simple channel flow to an industrially relevant application is presented. A non-equidistant grid resolution for LES simulations is used for the channel flow at a Reynolds

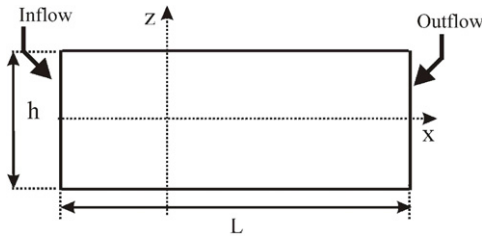

Fig. 1. Top view: computational domain in the xz-plane with dimensions, length $L = 200$ and width $b = 32$.

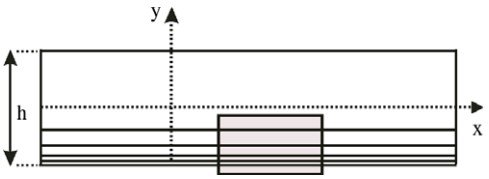

Fig. 2. Side view: calculation domain in the xy-plane with dimension, height $h = 48$. The shaded box is enlarged in Fig. 3 but in a different scaling.

Table 1
Domain dimensions.

Grid	h_0	h_1	h_2	h_3	h_4	h_5
Fine	0	21	1.75	0.875	0.25	0.125
Medium	10	12.25	1	0.5	0.25	0
Coarse	20	2.25	1	0.5	0.25	0

number of 6876, and the wall-mounted cube test case is considered for Reynolds numbers up to 40,000 with respect to the cube height.

4.1. Channel flow at Reynolds number 6876

Turbulent channel flows are standard test cases for wall-bounded flows. In the context of this work, a turbulent channel flow at a Reynolds number of 395 with respect to the friction velocity and half of the channel width is investigated and compared with DNS simulations published by Moser [5]. The test case allows for the investigation of the turbulent viscosity in a simple geometry. Here, the near-wall distance y^3 law is studied in detail.

4.1.1. Computational mesh

Investigations of the near-wall boundary layer require a high resolution. In order to save computational time and memory, the grid is successively coarsened with increasing distance from the wall. The dimensions of the channel are presented in Figs. 1 and 2. In order to determine the influence of the boundary layer resolution, three setups with different resolutions are examined. For the finest grid resolution, the wall is refined by five levels, so the wall cell spacing is $\frac{1}{16}$ of the size of cells in the center of the channel (Fig. 3). The dimensionless wall distances are $y_+ = 0.51$ for the finest grid resolution and $y_+ = 1.02$ for the medium and coarse grid resolutions. The distance y_+ is defined as: $y_+ = \frac{u_* y_1}{\nu_0}$, where u_* is the friction velocity at the nearest wall node, and y_1 is the distance to the nearest wall node.

The different grid resolutions are shown in Table 1. The values correspond to the dimensions of the coarsest grid cells. For each grid resolution, statistics from the coarsest grid cells over 40,000 time steps are used to derive the value of the averaged velocity component u.

4.1.2. Initial conditions

The main velocity component u runs parallel to the wall and is initialized according to Reichardt's law [15]:

$$U_R(y) = u_\tau U_R^+(y_+) \tag{25}$$

with

$$U_R^+(y_+) = \frac{1}{\kappa}\ln(1 + 0.4y_+) + 7.8\left[1 - e^{\frac{-y_+}{11}} - \frac{y_+}{11}e^{\frac{-y_+}{11}}\right] \tag{26}$$

where $\kappa = 0.41$ is the Karman constant and u_τ is the friction velocity.

The values calculated for the initial velocity U_R^+ are compared with those from the DNS data of Moser [5], as shown in Fig. 4. Inlet and outlet boundary conditions are periodic. The top boundary in Fig. 2 is a wall, and the other boundaries are symmetric. This means that the velocity gradient at the boundary is zero. In this test case, the LES Smagorinsky model constant is set to $C_S = 0.05$.

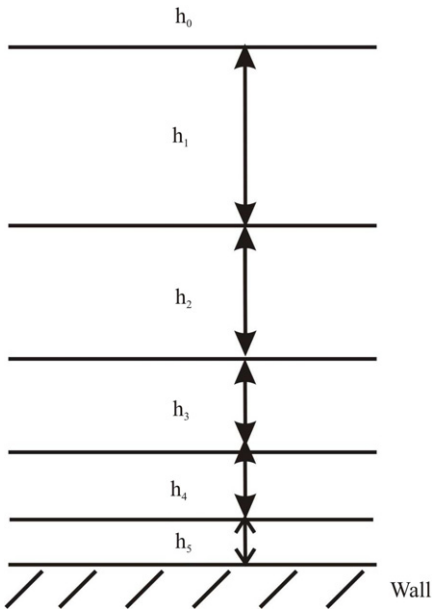

Fig. 3. Local grid refinement next to the wall.

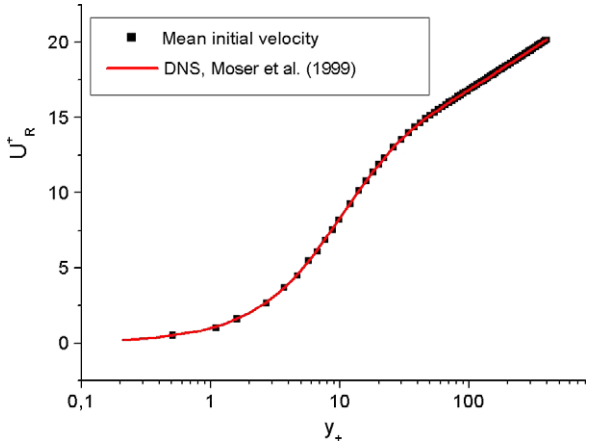

Fig. 4. Initial velocity profile u in the LB simulation compared with the DNS data from Moser [5].

A random velocity distribution with a maximum amplitude of one percent is added to the initial velocity in the whole domain. The pressure field is initialized using the LES WALE results obtained on the finest grid after 40,000 time steps, where the pressure field is not initialized. In this way, fewer time steps are needed before starting the averaging process. Only 10,000 time steps are required with this method to observe a fully developed turbulent flow, after which the time averaging procedure is carried out over 40,000 time steps.

4.1.3. Numerical results

LES WALE, Smagorinsky and Smagorinsky–Van Driest models are compared with the DNS simulation from Moser et al. [5]. Fig. 5 illustrates the behavior of the averaged dimensionless velocity u_+ versus the dimensionless wall distance y_+ for the finest grid resolution. Since the WALE model gives the correct near-wall scaling of y_+^3, the obtained data set corresponds to Moser's DNS data. Smagorinsky's model, as well as the Smagorinsky–Van Driest model, differs significantly from the DNS simulation. One reason for this is the near-wall scaling is not correctly reproduced. Specifically, the Smagorinsky model has a near-wall scaling of y_+, and the Smagorinsky–Van Driest model has a near-wall scaling of y_+^2.

In Fig. 6, the deviatoric diagonal Reynolds stress $\overline{u'u'}^* = \overline{u'u'} - \frac{1}{3}(\overline{u'u'} + \overline{v'v'} + \overline{w'w'})$ is plotted against the wall distance for the various LES models considered. The curves deviate only slightly from the DNS results.

To compare the grid resolutions, Figs. 7 and 8 present the results from the LES models for the medium and the coarse grid setups, respectively.

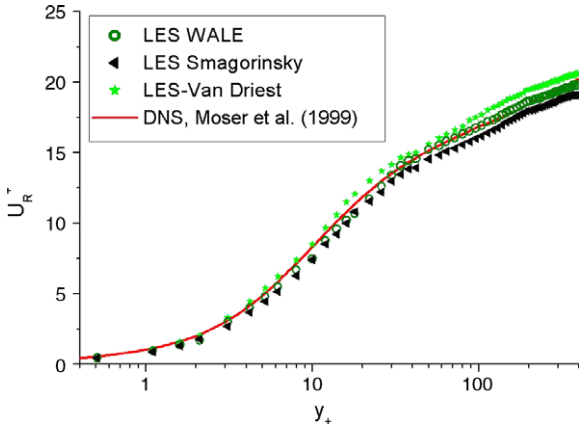

Fig. 5. Averaged main velocity component u on the finest grid resolution for a period of 40,000 averaged time steps. The three different SGS models: LES WALE, LES Smagorinsky and LES Van Driest are compared.

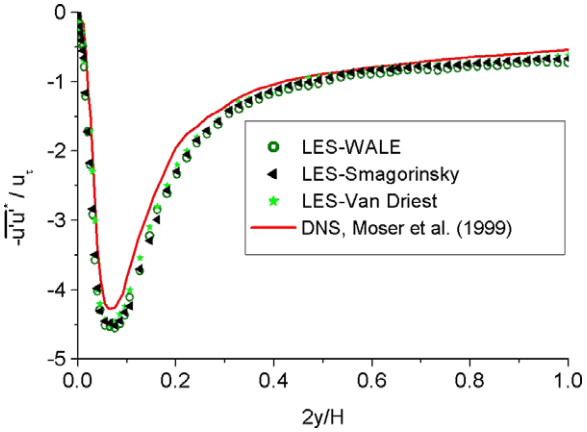

Fig. 6. Streamwise velocity fluctuation on the finest grid for a period of 40,000 time steps. The three different SGS models: LES WALE, LES Smagorinsky and LES Van Driest are compared. No significant deviations within the LES models are found. There is a slight discrepancy between the LB method and the DNS data near the boundary layer.

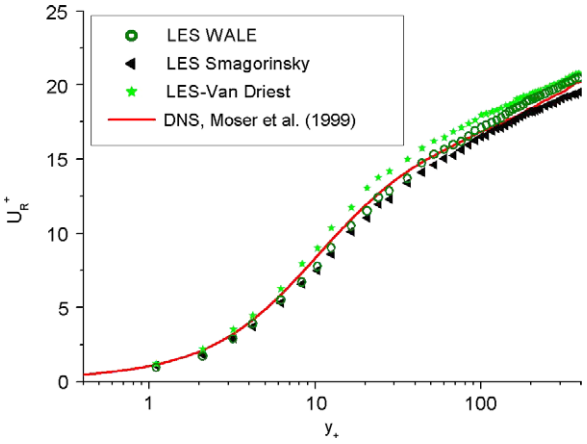

Fig. 7. Averaged main velocity component u on the medium grid for a period of 40,000 averaged time steps. The three different SGS models: LES WALE, LES Smagorinsky and LES Van Driest are compared.

With a finer grid resolution, the LES simulations converge to the DNS simulation for $y_+ < 100$. However, it is found that the LES Smagorinsky and the LES Van Driest models tend to converge to a shifted value of the velocity U_R^+ for $y_+ > 100$ (Fig. 5).

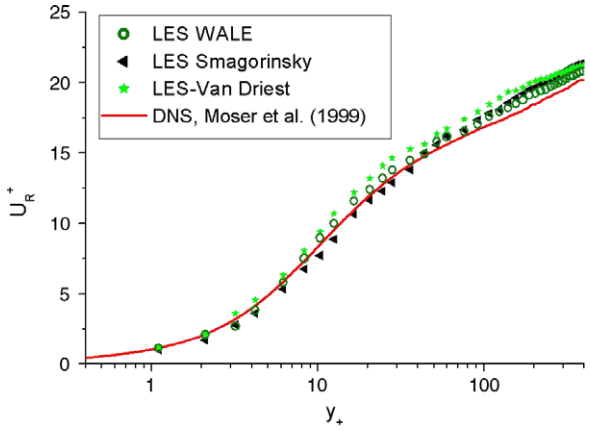

Fig. 8. Averaged main velocity component u on the coarse grid for a period of 40,000 averaged time steps. The three different SGS models: LES WALE, LES Smagorinsky and LES Van Driest are compared.

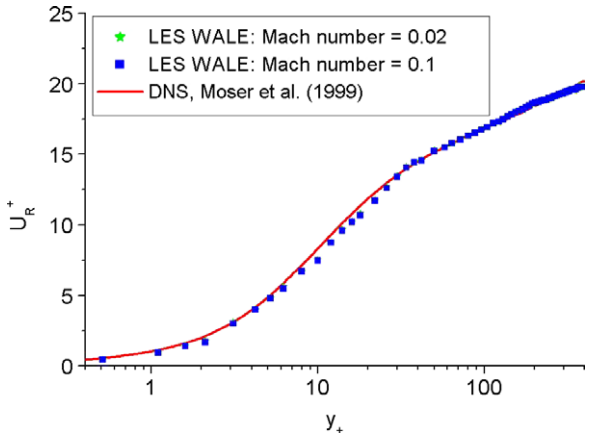

Fig. 9. Mach number influence on the fine grid. The Mach number 0.1 is compared with the Mach number 0.02 for a period of 40,000 averaged time steps.

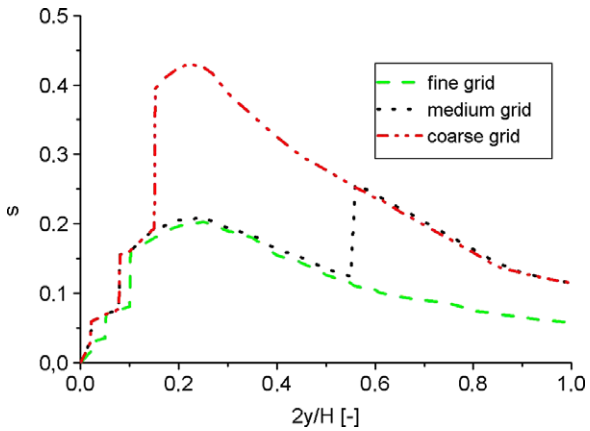

Fig. 10. Vertical profile of the activity parameter for different grid levels. The stepwise grid coarsening by a factor of 2 leads to a jump in the activity parameter.

For further investigation, simulations at two Mach numbers (Ma) are run. No significant deviation is observed between the values of U_R^+ for the respective cases at Mach numbers 0.1 and 0.02 in Fig. 9. The Mach number is defined as: $Ma = \frac{u}{c}$, where c denotes the speed of sound. To demonstrate the dependence of the sub-grid model on the grid, the activity parameter [16] for all three resolutions is plotted in Fig. 10. The activity parameter is defined as the ratio of the turbulent

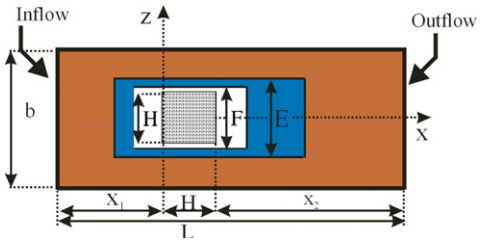

Fig. 11. Computational domain in the *xz*-plane with length $L = 256$ and width $b = 96$. White: fine grid size, dark grey: medium grid size; light grey: coarsest grid.

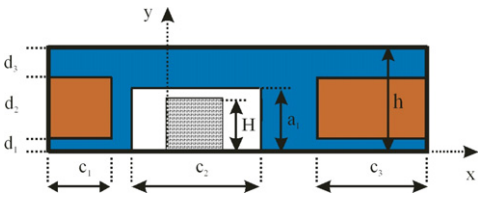

Fig. 12. Computational domain in the *xy*-plane with length $L = 256$ and height $h = 64$. White: fine grid size, dark grey: medium grid size; light grey: coarsest grid.

Table 2
Domain dimensions.

a_1	b	c_1	c_2	c_3	d_1	d_2	d_3
40	96	40	64	80	6	52	6
E	F	h	H	L	x_1	x_2	
42	36	64	32	256	64	160	

dissipation to the total dissipation:

$$s = \frac{\epsilon_t}{\epsilon_t + \epsilon_\mu} \tag{27}$$

with

$$\epsilon_t = \mu_t 2 S_{ij} \frac{\Delta u_i}{\Delta x_j}$$
$$\epsilon_\mu = \frac{1}{Re_\tau} S_{ij} \frac{\Delta u_i}{\Delta x_j}. \tag{28}$$

This ratio can be used to estimate the contribution of SGS modelling in LES compared with DNS. The grid coarsening leads to a jump in the activity parameter.

4.2. Wall-mounted cube test case for Reynolds numbers from 200 to 2,000

In various applications, obstacles within a channel flow can be of interest. Unfortunately, there are no universal predictions of the development of turbulent flows. The presented test case investigates the transition from laminar to turbulent flow conditions. For comparison, simulations are performed on an unstructured grid using the CFD code ANSYS CFX 11 [7]. Here, the Scale Adaptive Turbulence model (SAS) [6] is used. The advantage of the SAS simulation is that according to local space and time resolution, the solution corresponds to solutions from RANS, LES, or even DNS simulations.

4.2.1. Computational domain

For the lattice Boltzmann simulations up to Reynolds number 800, one local grid refinement is used around the wall-mounted cube. In this test case, the whole area consists of 4.2 million nodes. For higher Reynolds numbers, the cube is resolved with one additional finer grid level. In that case, the whole area will consist of 9.8 million nodes. A maximum y_+ value of 1.8 in the whole fluid domain is achieved. Figs. 11 and 12 illustrate the *xz*-plane and the *xy*-plane. The grey area shows the coarsest discretization with $\Delta x = 1 \times 10^{-6}$ m. Areas in shaded grey and white indicate one and two grid refinement levels, respectively. The dimensions of the flow domain are summarized in Table 2 in units of coarse grid cells.

Time averaging is started after 15,000 time steps. The velocity components are then averaged over 40,000 time steps. In the CFX simulation, the walls are resolved with an unstructured grid for all Reynolds numbers. The maximum y_+ value in the whole domain is 1.0, and for all Reynolds numbers, the boundary layer is resolved with at least 10 fluid nodes. In this test case, the LES Smagorinsky model constant C_S is set to 0.16.

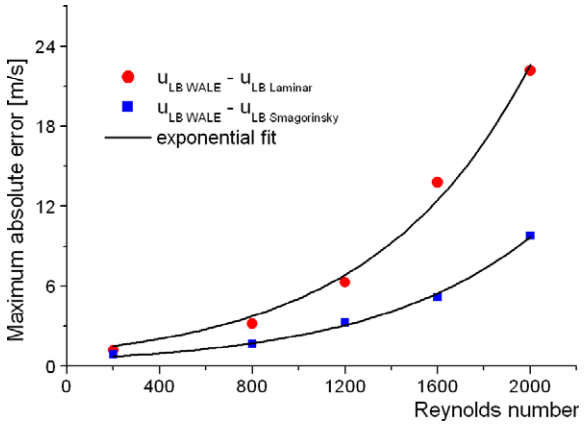

Fig. 13. Maximum deviations between the LES models for Reynolds numbers between 200 and 2000.

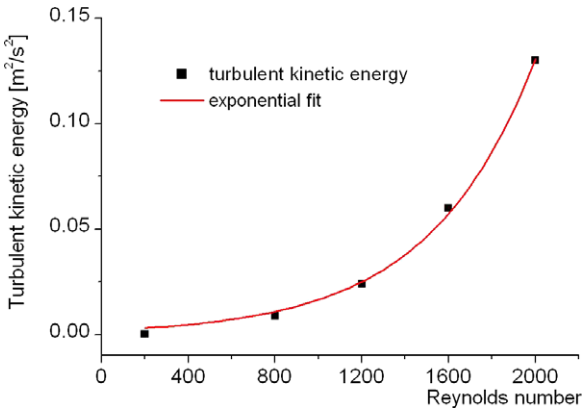

Fig. 14. Increase in the turbulent kinetic energy for Reynolds numbers between 200 to 2000.

4.2.2. Initial conditions

The initial velocity field is set via Reichardt's law (Section 4.1.2). The maximum lattice Boltzmann velocity at the inlet is 0.1. The outlet boundary condition is chosen in such a way that the velocity gradient in the direction normal to the outlet surface is zero. The bottom and side boundaries are treated as solid walls with the no-slip condition.

4.2.3. Numerical results

One possible way to measure the influence of the chosen LES model on the result is by analyzing the deviations that are obtained in the velocity component u between the different LES models. The deviations in the velocity component u increase exponentially with increasing Reynolds numbers, as shown in Fig. 13.

The exponential increase in turbulent kinetic energy with increasing Reynolds numbers (Fig. 14) gives a reasonable explanation for this phenomenon.

For position 1, directly in front of the cube ($x = 63.75\ \mu m, z = 0\ \mu m$), and position 2, one cube length behind the cube ($x = 128.0\ \mu m, z = 0\ \mu m$), Figs. 15–18 show the averaged velocity components for a Reynolds number of 2000 for the three LES models compared with the CFX SAS Simulation. Differences between the LES lattice Boltzmann simulation and the highly resolved CFX SAS Simulation at position 1, directly in front of the cube, are not significant.

At position 2 (behind the cube), no significant deviations are found between the lattice Boltzmann WALE simulation and the highly resolved CFX SAS simulation. The Smagorinsky model, however, shows significant differences in the averaged orthogonal velocity component v.

4.2.4. Computational effort

The computational time required for the LB WALE simulation at a Reynolds number of 2000 is approximately 206 CPU seconds for a full propagation step over the fluid cell using the maximum Courant Number of 0.14. For the CFX SAS simulation, the computational time amounts to 2,600 CPU seconds for a full propagation step over the same fluid cell. Both computational times are obtained using a single processor (AMD Athlon 3 GHz).

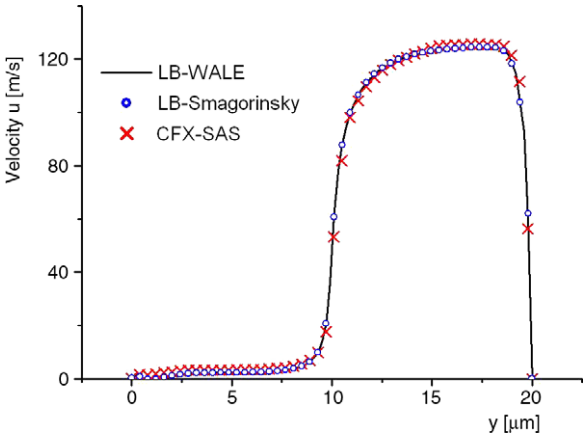

Fig. 15. Vertical profiles at position 1: Averaged main velocity component u for a period of 40,000 averaged time steps at Reynolds number 2000.

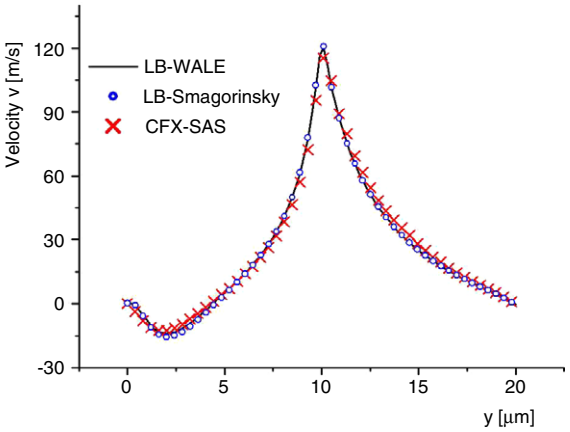

Fig. 16. Vertical profiles at position 1: Averaged velocity component v (orthogonal to the main velocity direction) for a period of 40,000 averaged time steps at Reynolds number 2000.

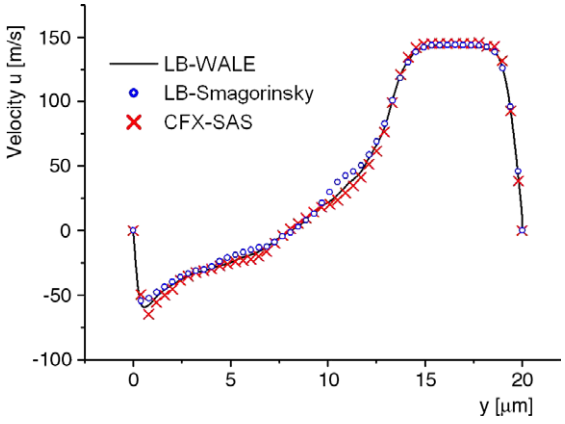

Fig. 17. Vertical profile at position 2. Averaged main velocity component u for a period of 40,000 averaged time steps at Reynolds number 2000.

4.3. Wall-mounted cube test case at a Reynolds number of 40,000

For this Reynolds number, a fully turbulent flow field is expected. The computational domain is enlarged and adapted to the experimental setup. In this test case, the LES Smagorinsky model constant C_S is set to 0.16.

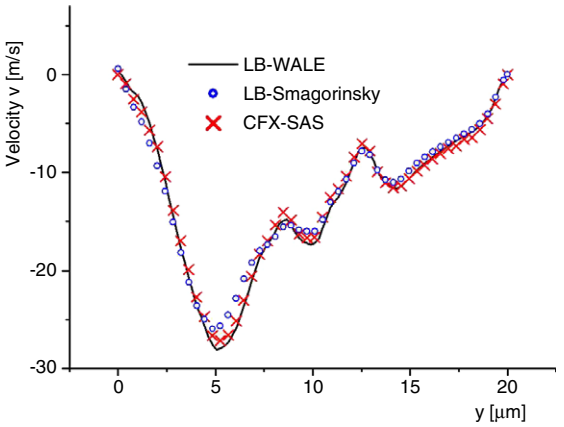

Fig. 18. Vertical profile at position 2. Averaged velocity component v (orthogonal to the main velocity direction) for a period of 40,000 averaged time steps at Reynolds number 2000.

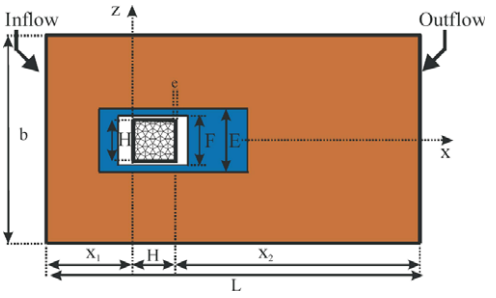

Fig. 19. Calculation domain in the xz-plane with length $L = 320$ and width $b = 224$. White: fine grid size, dark grey: medium grid size; light grey: coarsest grid.

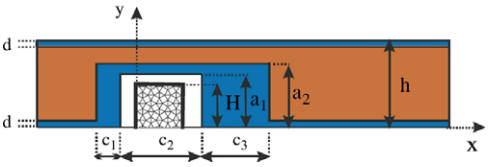

Fig. 20. Computational domain in the xy-plane with length $L = 256$ and height $b = 64$. White: fine grid size, dark grey: medium grid size; light grey: coarsest grid.

Table 3
Domain dimensions.

a_1	a_2	b	c_1	c_2	c_3	d	e
36	42	224	20	48	40	6	2
E	F	h	H	L	x_1	x_2	
44	38	64	32	320	96	192	

4.3.1. Computational domain

The mesh has two refinement levels around the wall boundaries. The coarsest grid has a discretization size of $\Delta x = 0.78125$ mm. The domain is resolved with 16.4 million nodes. The dimensions of the channel are illustrated in Figs. 19 and 20. The grey shadings indicate the same scales used in Section 4.2.

Again, the values in Table 3 correspond to the number of coarse grid cells. After 20,000 time steps, the velocity components are averaged over 60,000 time steps. Depending on the grid resolution, turbulent eddies next to the cube may be completely resolved. In that case, results would correspond to a DNS simulation. Eddies smaller than the grid resolution are covered with the LES fine structure model.

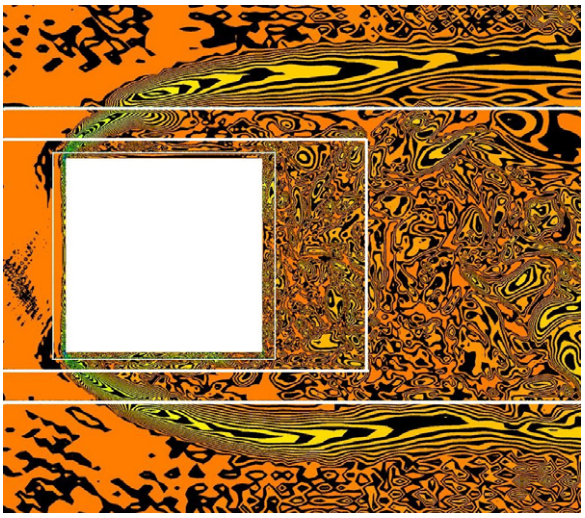

Fig. 21. Fluctuations in the streamwise velocity component in the xz-plane at $y = \frac{h}{3}$. The boundary between fine and medium grid sizes is indicated with a white line.

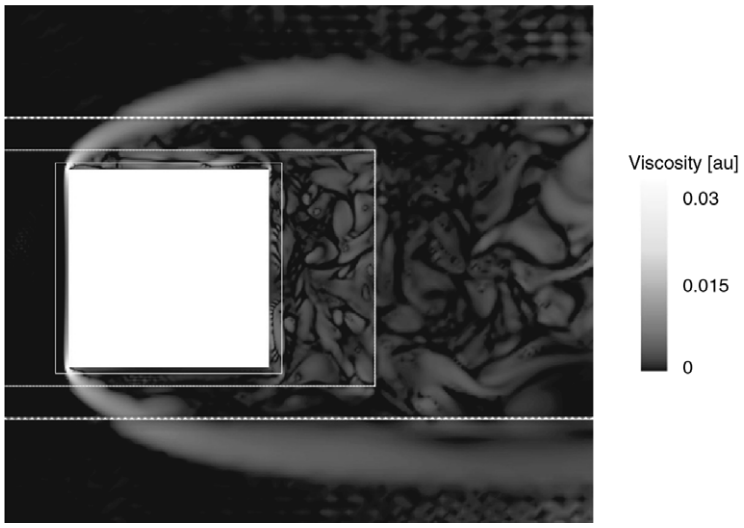

Fig. 22. Turbulent viscosity in the xz-plane at $y = \frac{h}{3}$. The white line indicates the boundary between the different grid resolutions.

4.3.2. Initial conditions

The velocity field is initialized by Reichardt's law (see Section 4.1.2). For the top, bottom, and side boundaries, solid walls with the no-slip condition are used. The outlet boundary condition is chosen in the same way as in Section 4.2.2, where the velocity gradient in the direction normal to the outlet surface is zero.

4.3.3. Numerical results

Fig. 21 shows the small eddies in the viscous boundary layer next to the cube in the xz-plane at $y = \frac{h}{3}$.

Depending on the grid resolution in Fig. 21, the minimum size of the resolved eddies varies. The turbulent viscosity is plotted in Fig. 22, in order to show its magnitude in the vicinity of the walls. The white lines symbolize the interface between the single grid resolution levels.

4.3.4. Validation

The averaged main velocity component u divided by the bulk velocity $u_b = 24.0\frac{m}{s}$ is compared with the experimental data from Martinuzzi [8] at the location directly above the cube (Fig. 23) and four cube lengths behind the cube (Fig. 24). The LES WALE simulation is found to match the experimental data better than the Smagorinsky model. The Smagorinsky–Van Driest model was not applied because the effort for the universal calculation of the local y_+ distances of arbitrary geometries is too expensive.

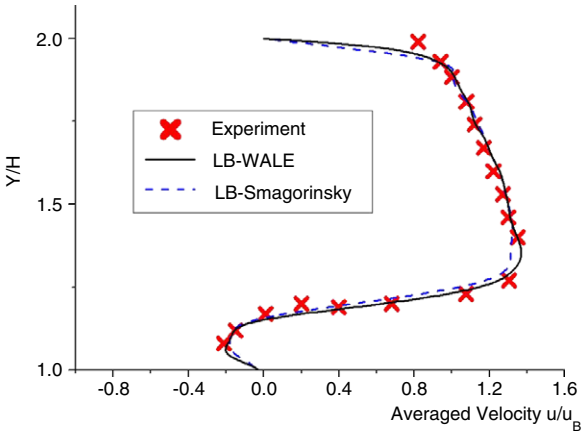

Fig. 23. Comparison of the velocity profile at $x = \frac{7l}{20}, z = 0\ \mu\text{m}$.

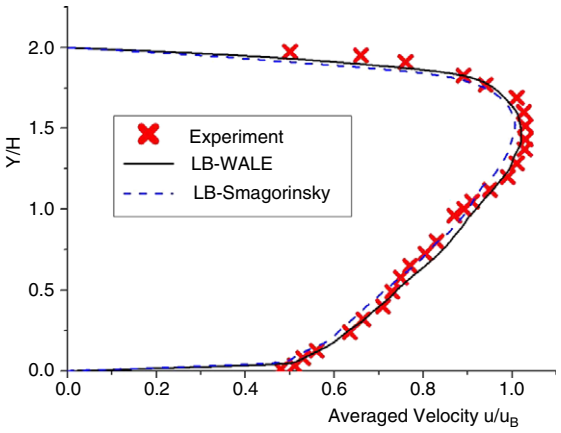

Fig. 24. Comparison of the velocity profile at $x = \frac{4l}{5}, z = 0\ \mu\text{m}$.

5. Conclusions

The implementation of the LES WALE model within the lattice Boltzmann framework presents advantages over the Smagorinsky model with or without damping functions. Furthermore, the LES WALE model follows the near-wall distance y^3 law, unlike the LES Smagorinsky model. As a consequence, this study reveals that the LES WALE model is more suitable for the presented channel flows, both with and without a wall-mounted cube. The local grid refinement reduces the computational effort and enables the capturing of the boundary layer. The physical process can be calculated with lattice Boltzmann methods as well as with finite volume schemes [1].

The LES models applied on the lattice Boltzmann scheme give very similar results to the finite volume methods that solve the Navier–Stokes equations. The numerical effort of these test cases is very high due to the fact that a large number of nodes is necessary for channel flows when applying the lattice Boltzmann equation on a Cartesian grid. Recently, approaches have been made to solve the lattice Boltzmann equation with a finite volume scheme [17]. Therefore, computation on unstructured grids might be possible in the future.

References

[1] I. Wendling, Dynamische large eddy simulation turbulenter Strömungen in komplexen Geometrien, Dissertation TU Darmstadt, 2007.
[2] F. Nicoud, F. Ducros, Subgrid-scale stress modelling based on the square of the velocity gradient tensor, Flow, Turbulence and Combustion 62 (1999) 183–200.
[3] J. Smagorinsky, General circulation experiments with the primitive equations I. The basic experiment, Monthly Weather Review 91 (1963) 99–164.
[4] D. Lilly, A proposed modification of the Germano subgrid-scale closure method, Physics of Fluids A 4 (1992) 633–635.
[5] R. Moser, J. Kim, N. Mansour, Direct numerical simulation of turbulent channel flow up to $Re_\tau = 590$, Physics of Fluids 11 (1999) 943–945.
[6] Y. Egorov, F. Menter, A scale adaptive simulation model using two-equation models, in: 43rd AIAA Aerospace Sciences Meeting and Exhibit, Reno, Nevada, 2005.
[7] ANSYS release 11.0 documentation, 2008. Available on www.kxcad.net/ansys/ANSYS/ansyshelp/ansys.set.html.
[8] R. Martinuzzi, Experimentelle Untersuchung der Umströmung wandgebundener, rechteckiger, prismatischer Hindernisse, Dissertation, Universität Erlangen, 1992.

[9] D. d'Humières, I. Ginzburg, M. Krafczyk, P. Lallemand, L.-S. Luo, Multiple-relaxation-time lattice Boltzmann models in three dimensions, The Royal Society 360 (2002) 437–451.
[10] B. Crouse, Lattice Boltzmann Strömungssimulationen auf Baumdatenstrukturen, Dissertation, TU München, 2003.
[11] S. Hou, et al., A lattice Boltzmann subgrid model for high Reynolds number flows, Fields Institute Communications 6 (1996) 151–165.
[12] M. Krafczyk, J. Tölke, L.S. Luo, LES simulations based on a multiple relaxation time LB model, International Journal of Modern Physics B 17 (2003) 33–39.
[13] M. Germano, U. Piomelli, P. Moin, W. Cabot, A dynamic subgrid-scale eddy viscosity model, Physics of Fluids A 7 (1991) 1760–1765.
[14] P. Sagaut, Large Eddy Simulation for Incompressible Flows, Springer, 2006.
[15] H. Reichardt, Gesetzmässigkeiten der freien Turbulenz, VDI Forschungsheft 414 (1951).
[16] T. Brandt, A posteriori study on modelling and numerical error in LES applying the Smagorinsky model, in: Complex Effects in Large Eddy Simulation Limassol, September 20–24, 2005.
[17] H. Xi, G. Peng, S.H. Chou, Finite-volume lattice Boltzmann method, Physical Review E 59 (1999) 6202–6205.